Environmental Modelling and Software 156 (2022) 105473

Contents lists available at ScienceDirect

Environmental Modelling and Software

journal homepage: www.elsevier.com/locate/envsoft

The Dynamic Temperate and Boreal Fire and Forest-Ecosystem Simulator (DYNAFFOREST): Development and evaluation

Winslow D. Hansen [a,*], Meg A. Krawchuk [b], Anna T. Trugman [c], A. Park Williams [d,e]

[a] Cary Institute of Ecosystem Studies, Millbrook, NY, 12545, USA
[b] College of Forestry, Oregon State University, Corvallis, OR, 97331, USA
[c] Department of Geography, University of California, Santa Barbara, CA, 93016, USA
[d] Department of Geography, University of California, Los Angeles, CA, 90095, USA
[e] Lamont-Doherty Earth Observatory, Columbia University, Palisades, NY, 10964, USA

ARTICLE INFO

Keywords:
Climate change
Ecosystem modeling
Forest resilience
Natural disturbance
Scaling
Wildfire

ABSTRACT

Fire is a dominant disturbance in temperate and boreal biomes, and increasing burned area with climate change may fundamentally alter forests. Improved information about how fire-induced changes to forests may feedback to affect subsequent burning at regional scales could inform forest management and climate-mitigation strategies. However, fire is simplistically represented in Earth System Models, and regional statistical fire models often assume sufficient fuels, contributing to uncertainty in future projections. To address this challenge, we developed the Dynamic Temperate and Boreal Fire and Forest-Ecosystem Simulator (DYNAFFOREST). DYNAFFOREST represents the hierarchical structuring of forests, from individual cohorts to continental extents, making it possible to simulate feedbacks between fire and forests at broad scales over decades to centuries. We parameterized DYNAFFOREST for the western United States of America and benchmarked simulations with observations. DYNAFFOREST recreated patterns of forest cover, structure, and downed fuels, and was capable of capturing average 20th-century fire activity.

1. Introduction

Forest fire is a prevalent natural disturbance in terrestrial ecosystems and is sensitive to climate, particularly in temperate- and boreal-forest biomes (Seidl et al., 2020). Trends toward warmer, more arid conditions are causing fire frequency, size, and severity to rapidly increase in many places (Abatzoglou and Williams, 2016; Kelly et al., 2013; Westerling, 2016). For example, annual burned forest area has grown ~1,100% since 1984 in the western conterminous United States of America (hereafter; western US) (Williams et al., 2022). Current climate-fire trends will almost certainly continue over the next few decades (Abatzoglou et al., 2021) with large consequences for people and ecosystems (Coop et al., 2020; McWethy et al., 2019; Schoennagel et al., 2017). While climate is a dominant cause of increasing fire activity, other factors also contribute to recent trends, including spatiotemporal variability in fuel loads sometimes related to legacies of fire suppression, and human-caused ignitions (Balch et al., 2017; Calef et al., 2008; Hagmann et al., 2021). Many of these drivers are not well accounted for in disturbance-succession models of forests, particularly at broader scales, nor are the complex feedbacks between fire and its drivers. Therefore, new quantitative tools that incorporate multiple drivers and feedbacks could yield important insights into the trends, causes, and consequences of forest fire.

One of the most important feedbacks that models must better capture is how fires can alter forests in ways that affect the likelihood of subsequent burning. Two pathways exist through which these fire-forest feedbacks play out. First, fire combusts fuels, which decreases the probability of another fire for a period. In the western US, reduced fire probability can last 5–30 years after the initial burn, depending on climate and extreme weather events (Parks et al., 2018). Second, increased burning can initiate transitions from forests to alternate vegetation communities that differ in their flammability (Johnstone et al., 2016; Tepley et al., 2018). For example, less flammable deciduous tree species now commonly replace black spruce after unusually severe fire in the North American boreal forest. Scientists and practitioners need improved information about where, when, and why fire-induced changes to forests may feedback to affect subsequent burning, otherwise known as re-burns (Prichard et al., 2017; Schoennagel et al., 2017).

* Corresponding author.
E-mail address: hansenw@caryinstitute.org (W.D. Hansen).

https://doi.org/10.1016/j.envsoft.2022.105473
Received 20 October 2021; Received in revised form 17 April 2022; Accepted 21 July 2022
Available online 31 July 2022

This need for improved modeling is particularly true across regional to continental scales (Becknell et al., 2015; Turetsky et al., 2017; Walker et al., 2018); the spatial scales at which policy and management are commonly targeted and impending ecological change could alter broader Earth-system functions (Heffernan et al., 2014; Rose et al., 2017).

Most models capable of simulating broad spatial domains ($\geq 10^6$ km^2) ignore or simplistically represent fire and/or do not explicitly represent forests and their dynamics. For example, Earth System Models (ESMs) were designed to simulate the role of vegetation in regional-to global-carbon and water cycling, but have a coarse spatial resolution ($\geq 0.5°$) and often do not include fire (Hantson et al., 2020; Rabin et al., 2017). Of the few ESMs with a dynamic fire module, most only simulate aggregate burned area and do not include the demographic processes that underpin forest recovery, like tree-seed dispersal and seedling establishment (Fisher et al., 2018; Hantson et al., 2020; Sanderson and Fisher, 2020). At regional scales, statistical models of fire are often used that operate at a finer spatial grain (~6–12 km) and represent the multi-step process of burning more realistically than ESMs by relating observed climate to individual fire characteristics, such as occurrence, size, and severity (Keyser and Westerling, 2019; Westerling et al., 2011). However, statistical fire models rarely simulate forest change, and assume sufficient fuel and unchanging forest cover when projecting future fire, use rules to define the duration after a fire in which a cell cannot burn, employ empirical functions to implicitly represent dynamic patterns of postfire fuel limitation, or implement simple statistical vegetation-climate relationships to represent potential change in fuels with climate (Abatzoglou et al., 2021; Kitzberger et al., 2017; Littell et al., 2018). Numerous forest-landscape models include both fire and detailed representations of forest dynamics. Such models capture the necessary demographic processes and simulate feedbacks to fire (Albrich et al., 2020; Hansen et al., 2020; Hurteau et al., 2019; Seidl et al., 2014; Serra-Diaz et al., 2018), but are computationally expensive, and most cannot be run for broad domains (though see Rammer and Seidl, 2019).

To address the dearth of quantitative tools capable of modeling temperate and boreal fire and forests across regions to continents, we present a new model called the **DYNA**mic Temperate and Boreal **F**ire and **FOR**est-**E**cosy**ST**em simulator (DYNAFFOREST). We designed DYNAFFOREST to simulate complex and interacting causes of fire and to represent the demographic processes that underpin postfire forest recovery. Thus, the model is capable of simulating dynamic feedbacks between fire and forests. DYNAFFOREST is computationally efficient such that it can be run with a sufficiently fine spatial resolution (1-km) to capture heterogeneity in vegetation size classes, structure, and stand ages in topographically complex landscapes. The model is capable of simulating broad domains of similar scope to the forested area of the western US; ~850,000 km^2 and operates at an annual time step. In this paper, we describe DYNAFFOREST and evaluate model skill by comparing simulations of western US forests under mid-20th century climate conditions with multiple independent benchmarking datasets.

2. Materials and methods

2.1. Model overview

Our objective was to represent how forest fires and climate affect temperate- and boreal-forest ecosystems across regions to continents,

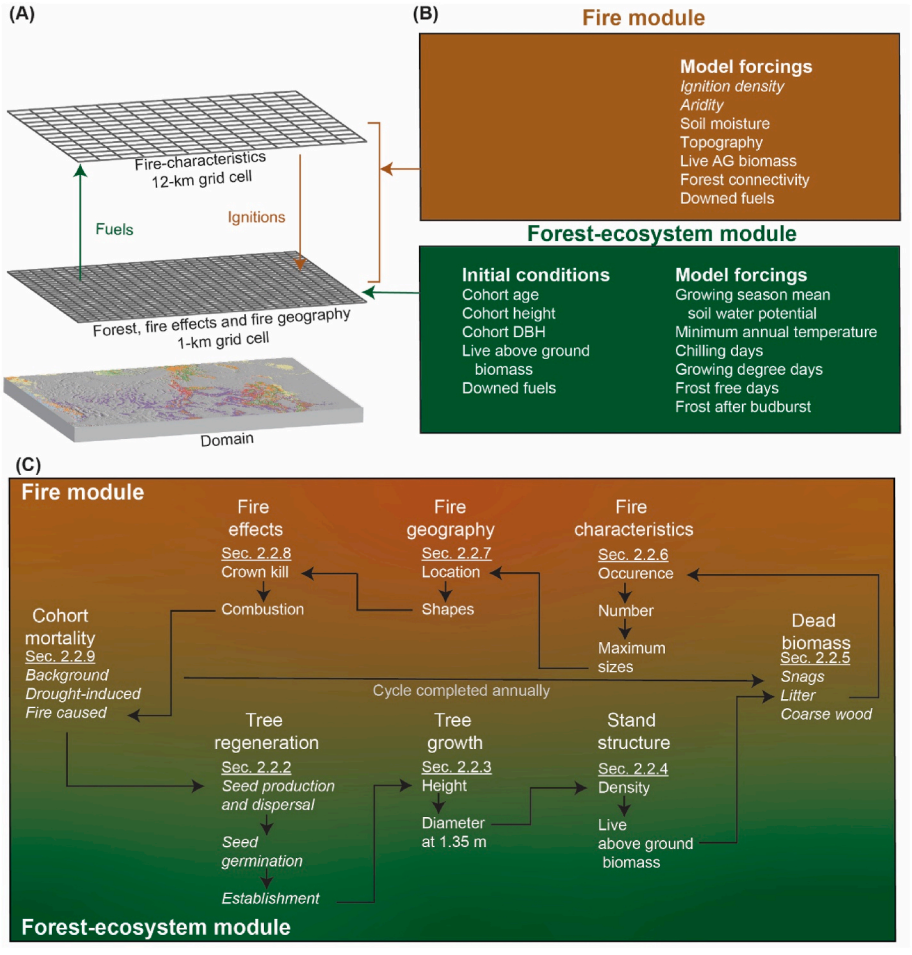

Fig. 1. DYNAFFOREST simulates dynamic interactions and feedbacks between fire and forest ecosystems in temperature and boreal biomes. (A) Spatial resolution of processes represented in the fire and forest-ecosystem modules. (B) Initial conditions and model forcing variables for the fire and forest-ecosystem modules. Italicized text differentiates variables that were the climatological mean from those that varied annually during model benchmarking for the western US. (C) Schematic of the processes represented in DYNAFFOREST. Italicized text differentiates model components that are probabilistic and process-based from those that are deterministic based on successional stage.

and how fire-induced changes to forests feedback to alter subsequent fires. DYNAFFOREST is broken into two modules: a forest-ecosystem module and a fire module (Fig. 1). We constructed DYNAFFOREST with a hierarchical structure where the forest-ecosystem module operates at a 1-km spatial resolution, and the fire module operates at a 12-km resolution. The time step of both modules is annual.

The forest-ecosystem module probabilistically represents key processes through which fire and climate affect forests and uses deterministic equations to represent other forest processes based on age/successional stage (Fig. 1C). Forest types can be parameterized at the level of specificity necessary for the application, from individual species to coarse plant functional types (PFTs). We simulate broad spatial domains with a fine grain size using a cohort-based approach that tracks a single cohort for each 1-km grid cell. The cohort has an age-dependent size and density based on PFT-specific traits. The approach is computationally efficient, as only one cohort per grid cell must be tracked. It also still allows for representation of heterogeneity in forest cover, composition, and structure at a 1-km resolution, which is finer than other models capable of simulating forests across comparable domains (Buotte et al., 2018; Fisher et al., 2018). However, because one PFT cohort per grid cell is tracked, the model does not explicitly represent relay successional trajectories, where transitions from the initial fast growing pioneer tree species (or shrubs) to slow growing late successional shade-tolerant species may alter stand flammability with time since disturbance (e.g., Tepley et al., 2018). Probabilistic process-based components are inspired by and closely follow the forest model iLand (Seidl et al., 2012a), which has been widely applied in temperate and boreal forests (Braziunas et al., 2018; Hansen et al., 2018, 2020, 2021; Seidl et al., 2014). Deterministic components are derived from several sources (e.g., Dixon, 2015; Rammig et al., 2007). A technical description of the forest-ecosystem module is provided in sections 2.2–2.5, section 2.9, and Appendix S1.

We paired the forest-ecosystem module with a statistically based fire module that predicts the occurrence, number, and sizes of fires >100 ha as a function of variables including the amount and connectivity of fuels from the forest module, spatial variation in climate aridity, natural and human-caused ignitions, and topography (Appendix S1). The module is designed so users can parameterize it based on an *a priori* understanding of their own system. Fire occurrence, number, and maximum size are simulated on a grid with a spatial resolution of 12 km. Fires are then randomly ignited in a forested 1-km grid cell within the 12-km fire cell and iteratively spread to other forested 1-km grid cells, until no more forested cells remain, or the maximum size predicted by the fire module is reached. Fire effects, such as cohort mortality and combustion of live biomass and fuel loads, are calculated at the 1-km resolution of the forest-ecosystem module.

Because our goal in this initial development and presentation of DYNAFFOREST was to establish whether the approach could accurately simulate forest dynamics when dynamically coupled with a module that produced 20th-century fire seasons, the fire module implemented here does not include fire response to temporal climate variability. Instead, it represents responses of fire to spatiotemporal changes in forest biomass and spatial variations in long-term mean aridity and ignition sources. As such, it is inevitable that this relatively simple baseline fire module will under-represent the frequency of very large wildfires, which are strongly promoted by the extreme climate anomalies that have occurred more frequently in recent years with human-caused warming. A technical description of the fire module is provided in sections 2.2.6–2.2.8 and Appendix S1, along with next steps for future development.

Together, the forest-ecosystem and fire modules provide a powerful framework for addressing previously intractable questions about how feedbacks emerge to shape temperate- and boreal-forest and fire outcomes. The flexibility of the fire module means it can be adjusted to fit a wide range of applications. The forest-ecosystem module takes a unique approach, explicitly representing some key forest processes with great detail (e.g., tree regeneration and mortality) and deterministically representing others (e.g., tree growth and stand density). Parameters for the model (Table 1) can be attained from the literature and public databases for most study areas globally. DYNAFFOREST currently only represents fire, but other natural and human-caused disturbances, such as bark beetle outbreaks, restoration treatments, and logging, are also important in temperate and boreal forests (Berner et al., 2017; Morris et al., 2016; Ruess et al., 2021). The modular design of DYNAFFOREST makes it easy to develop or plug-in future modules representing other disturbance agents and management activities (Honkaniemi et al., 2021;

Table 1
Model parameter descriptions. dim = dimensionless, emp = empirical coefficient.

Parameter	Units	Description
Dispersal		
Reproductive age	Years	The age at which PFT is reproductively mature
Seed mass	mg	Average mass of seeds used in calculating fecundity
Germination rate	dim	Average rate of seed germination under optimal conditions used in calculating fecundity
Fecundity	Seedlings m^{-2}	The number of potential seedlings per square m of mature forest canopy
Seed kernel a	m	Parameter of the dispersal kernel
Seed kernel b	m	Parameter of the dispersal kernel
Seed kernel c	dim	Parameter of the dispersal kernel
Seedling establishment		
Min. temperature	°C	Minimum winter daily temperature that seeds can tolerate before germination
Chill requirement	days	Number of days since end of last growing season with daily temperature between −5 and 5 °C
Min. growing degree days	degree days	Number of growing degree days required for establishment
Max. growing degree days	degree days	Number of growing degree days seedlings can tolerate
Growing degree days before budburst	degree days	Number of growing degree days required for seedling bud burst
Frost free days	days	Number of days without frost required for regeneration
Frost tolerance	dim	Parameter for estimating frost damage
Min. soil water potential	MPa	Lowest soil water potential seedlings can tolerate
Tree growth		
Max. height	m	Maximum height a tree of a PFT can attain
Growth coefficient	dim	Parameter for the height growth equation
Height to diameter	dim	Parameter for estimating diameter at 1.35 m
Stand density		
Stand density Index	Trees ha^{-1}	Parameter for estimating stand density from DBH
Live biomass		
Stem biomass a	dim	Parameter for stem biomass allometric equation
Stem biomass b	dim	Parameter for stem biomass allometric equation
Branch biomass a	emp.	Parameter for branch biomass allometric equation
Branch biomass b	emp.	Parameter for branch biomass allometric equation
Leaf biomass a	emp.	Parameter for leaf biomass allometric equation
Leaf biomass b	emp.	Parameter for leaf biomass allometric equation
Tree mortality		
Probability of reaching max. age	dim	Parameter for background mortality equation
Maximum age	years	The maximum age a PFT commonly attains
Hydraulic safety margin	MPa	Minimum xylem water potential typically experienced and xylem water potential that cause a 50% loss of conductivity
Bark Thickness	dim	Parameter for estimating probability of tree mortality from fire ratio of bark thickness to total tree diameter

Rammer and Seidl, 2015).

2.2. Detailed model description

2.2.1. Technical implementation

We aimed to develop a model that is adaptable for a wide range of applications and useable by researchers with varying expertise in programming. Thus, we wrote DYNAFFOREST in the R language and environment for statistical computing (V. 4.0.4) (Core Team, 2021). While other programming languages offer superior computational efficiency (e.g., C++), many ecologists and environmental scientists are experienced with R, and the software is open source, making it an ideal choice for encouraging widespread use and rapid community-based evolution of the model. Full source code and documentation is available under a GNU General Public License (GNU GPL www.gnu.org/licenses/gpl-3.0.html).

2.2.2. Tree regeneration

Stem density and species composition of tree seedlings that establish after severe fire shape successional trajectories for decades to centuries (Kashian et al., 2005). Postfire tree regeneration can be compromised if fires recur before trees reach reproductive maturity (Brown and Johnstone, 2012; Buma et al., 2013), if the size of severely burned patches exceeds dispersal distance from the unburned edge or fire refugia (Gill et al., 2022), if winter snowpack or cold temperatures reduce germination rates (e.g., at high-elevation treeline; Brown et al., 2019; Kueppers et al., 2017), or if postfire drought kills tree seedlings (Davis et al., 2019; Hansen and Turner, 2019). Because tree regeneration is essential for postfire recovery, we took a probabilistic process-based approach.

Tree regeneration is simulated in DYNAFFOREST starting the year after a forest cohort dies from density independent mortality (factors related to tree age/size), fire, or drought, and continues annually until another cohort establishes or the simulation ends (Fig. 1C). Seed supply is modeled based on PFT-specific fecundity, which is the number of potential seedlings produced per m^2 of forest canopy and calculated using average seed mass, germination rate, and early seedling survival (Moles et al., 2004) (Appendix S1). Fecundity is assumed to be zero if a cohort is reproductively immature. If the cohort that died in the target cell was reproductively mature, we assume sufficient within-cell seed supply from that PFT to support regeneration in the year after cohort mortality (probability of dispersal equals 1), which allows us to implicitly account for surviving trees in the target grid cell and alternate regeneration strategies, such as asexual resprouting and cone serotiny. Even the largest and most severe 20th-century fires often generated mosaics of live and burned trees that ensured sufficient seed for regeneration in the year following fire (Harvey et al., 2016; Turner et al., 1997). Thus, we felt this assumption was warranted given our goal of simulating 20th-century forests and fire. However, fire severity is increasing with climate change such that seed limitation is a growing concern, and future projections with DYNAFFOREST will require explicitly simulating within-cell seed supply as a function of percent crown kill (Gill et al., 2022; Parks and Abatzoglou, 2020; Steel et al., 2018). We also calculate the probability of dispersal from PFTs in the eight directly adjacent grid cells using a two-part exponential equation (Seidl et al., 2012a) (Appendix S1).

Effects of temperature and drought on tree-seedling establishment are then simulated following a mechanistic approach commonly implemented in process-based forest models (Burton and Cumming, 1995; Hansen et al., 2018; Nitschke and Innes, 2008; Seidl et al., 2012a) (Fig. 1C). Annual establishment probability is calculated for each PFT with a non-zero probability of dispersal as a function of temperature thresholds. Annual seed stratification is assessed based on a PFT-specific chilling day requirement (# of days between −5 and 5 °C from the end of the previous growing season; defined as September 30th in our model). The coldest daily temperature during the year and the annual number of frost days (number of days below 0 °C) also cannot exceed PFT-specific thresholds. If germination requirements are met, climate effects on early seedling survival are assessed. Minimum and maximum annual growing degree day thresholds ensure appropriate growing-season length for seedlings to establish. Frost after bud burst and unusually dry soils jointly reduce probability of establishment representing frost-induced damage (Johnson et al., 2011) and drought-induced mortality (Hansen and Turner, 2019):

$$Estab.\ prob.ab_{g,t} = Frost.tol^{\sqrt{frost.after.bud_{g,t}}} * \frac{\left(PSI.AVE_{g,t} - PSI_{min}\right)}{\left(PSI_{field} - PSI_{min}\right)} \quad \text{Eq. 1}$$

where $Estab.\ prob.ab_{g,t}$ is the probability of establishment due to abiotic factors in grid cell g and year t, $Frost.tol$ is a PFT-specific frost tolerance parameter, $frost.after.bud_{g,t}$ is the number of frost days that occur after bud break in grid cell g and year t, $PSI.AVE_{g,t}$ is the mean growing season soil water potential in grid cell g and year t, PSI_{min} is the minimum soil water potential in which seedlings of a given PFT can establish, and PSI_{field} is the soil water potential at field capacity.

Probability of dispersal from the target and neighboring cells and probability of establishment are multiplied to calculate a total regeneration probability for each PFT. The PFT with the highest regeneration probability gets first priority for regeneration. We compare regeneration probability to a value between 0 and 1 randomly drawn from a uniform distribution. If probability of regeneration exceeds the random number, the PFT with highest priority regenerates. If not, another random number is drawn and compared to the PFT with the next highest regeneration probability. This continues until either any PFT with a nonzero regeneration probability is established or regeneration fails for all PFTs. If no new cohort establishes in the year following cohort mortality, grid cells are converted to a grassland/shrub-land/meadow ecosystem state (hereafter grassland), and the tree regeneration algorithms are called each year until a PFT regenerates or the simulation completes. The model is also capable of representing inhibition or facilitation of tree-seedling establishment by grasses and shrubs (Appendix S1).

2.2.3. Tree growth

Annual tree-height increment of each forest cohort is deterministically represented based on the prior year's height using a Bertalanffy growth equation (Von Bertalanffy, 1957) as adapted by Rammig et al. (2007) (Fig. 1C, Appendix S1). Height growth rate is PFT specific and not responsive to climate in our model. We then use a PFT-specific tree height-to-diameter ratio to derive tree diameter at a height of 1.35 m (DBH).

2.2.4. Stand structure

Temperate and boreal tree density often declines with stand age due to self-thinning from intraspecific competition. Stand density in DYNAFFOREST is estimated from DBH using empirical self-thinning relationships, also known as Reineke's R (Reineke, 1933) following an approach similar to the US Forest Service's Forest Vegetation Simulator (FVS) (Dixon, 2015) (Fig. 1C). Based on tree DBH and stand density, live biomass pools in stems, branches, and leaves are simulated with PFT-specific allometric equations. The leaf and branch biomass that dies and falls to the forest floor is also modeled with pool-specific turnover rates that can be set individually based on PFT-specific rates (Table 1).

2.2.5. Dead biomass

Falling leaves and branches are immediately added to dead forest floor biomass pools (Fig. 1C). The model tracks three pools of dead plant material in each grid cell: standing snags, forest-floor litter, and downed coarse wood. When a cohort dies from density independent mortality or drought (see section 2.2.9), all leaf and branch biomass is added to the forest floor litter and coarse wood pools in the following year. Standing snag biomass is added to the coarse wood pool over time based on a PFT-specific snag half-life (Seidl et al., 2012b; Stenzel et al., 2019). When a

cohort is burned, live leaf and branch pools are reduced proportional to percent crown kill (see section 2.2.9). Of the percent crown killed, we assume 90% of live leaf biomass and 50% of live branch biomass is combusted and emitted to the atmosphere (Seidl et al., 2014). The remainder is added to the litter and downed coarse wood pools. If a cohort is killed by fire, 100% crown kill is assumed for the purposes of calculating live-leaf and branch biomass combustion and turnover to dead forest floor pools. In the future, this could be expanded to also represent percent crown kill via heating and scorching. Snags fall and enter the coarse wood pool according to their PFT-specific half-life parameter. Following a fire, the portions of dead forest-floor fuel pools that were available for burning are assumed to be combusted, whether or not the forest cohort occupying the grid cell is killed, simulating surface fire in the stand (Seidl et al., 2014). Decomposition of each pool is calculated assuming a pool-specific decomposition rate that is invariant with climate.

2.2.6. Fire characteristics

The statistical fire module simulates fire characteristics at the resolution of 12-km grid cells. Before simulations can be run, the DYNAFFOREST fire module is parameterized in a flexible framework where regressions are constructed to separately predict fire occurrence, number, and size as a function of variables that can vary depending on *a priori* understanding of the study domain. We use model selection with AIC to determine the most skilled and parsimonious models. Appendix S1 provides an in-depth description of how the fire module was parameterized for forests of the western US.

First, DYNAFFOREST probabilistically predicts whether one or more fires has occurred, where the likelihood of fire increases as a function of variables like the amount and connectivity of fuels, aridity, and natural and human-caused ignition density (Fig. 1C):

$$FireProb_{g,t} = \frac{1}{1 + e^{(-(b_0 + b_1 * Predictor_1 + b_2 * Predictor_2 \ldots b_n * Predictor_n))}} \quad \text{Eq. 2}$$

where *FireProb* is the probability of at least one fire occurring in grid cell *g* and year *t*, and $Predictor_1$ through $Predictor_n$ are indices of fire probability selected in a stepwise multi-variable logistic regression (Appendix S1). If one or more fires are predicted in a grid cell, the module calculates the probability of different numbers of fires occurring based on:

$$Probfires_{n,g,t} = \frac{1}{1 + e^{\left(-\left(a + b * FireProb_{g,t}\right)\right)}} \quad \text{Eq. 3}$$

where $Probfires_{n,g,t}$ is the probability of *n* fires occurring in grid cell *g* and year *t* (*n* ranges from 1 to the maximum number of fires recorded in the simulation domain during the observational record), and *a* and *b* are empirical coefficients determined from logistic regression using $FireProb_{g,t}$ as a single predictor (Westerling et al., 2011). The number of fires is then probabilistically selected.

Maximum predicted size of each fire is determined based on an empirical stepwise multivariable regression that relates observed fire sizes to most of the same predictors used to estimate *FireProb* (Appendix S1). Rather than predicting maximum fire size directly, we predict cumulative distribution function (CDF) quantile values. We then randomly select a fire-size CDF value from the 200 observations in the empirical distribution that were closest to the predicted fire-size quantile and back transform to the maximum fire size by assuming that each region's fire sizes come from a generalized Pareto distribution. Thus, if multiple fires are predicted to occur in a grid cell, they can have different predicted maximum sizes despite identical predictor conditions. Maximum fire sizes can range from 100 ha up to the largest fire in the observational record, which can exceed a 12 km grid cell.

2.2.7. Fire geography

For each simulated fire, DYNAFFOREST randomly selects a forested 1-km grid cell from within the 12-km fire grid cell as the ignition point (Fig. 1C). Fire shapes are grown up to the predicted fire size using an algorithm where fires spread iteratively from the ignition point, burning all neighboring 1-km cells that are classified as forest ecosystem (i.e., grid cells that are forested or that are grassland but were initialized as forest) or that are nonforested lands immediately adjacent to grid cells classified as forest ecosystem. This allows us to account for forest fires that commonly spread through grasslands to another forest patch, and for spotting, where embers are carried in the air and set new fires. If sufficient fuels exist, fires can reach their maximum size predicted by climate, which can exceed the 12-km fire grid. However, complex shapes emerge because non-burnable grid cells may constrain fire spread, which can cause fires to not reach their maximum predicted size if there are insufficient connected grid cells to burn.

2.2.8. Fire effects

Tremendous variability exists in the severity of forest fires across temperate- and boreal-forest biomes, ranging from surface fires where mature trees survive, to severe stand-replacing crown fires that kill all trees. DYNAFFOREST simulates fire severity for each burned 1-km grid cell as percent crown kill (percent of the tree crown consumed by fire) following an approach commonly implemented in process-based forest models (Hansen et al., 2020; Schumacher et al., 2006; Seidl et al., 2014) (Fig. 1C).

$$CK_{g,t} = \min\left(KCK1 + KCK2 * DBH_{g,t} * Fuel_{g,t}\ , 1\right) \quad \text{Eq.4}$$

where $CK_{g,t}$ is the percent crown kill in burned grid cell *g* and year *t*. *KCK*1 and *KCK*2 are empirically derived parameters from the literature that describe how tree sizes and available fuels determine how much of the crown is killed by fire, and $Fuel_{g,t}$ is the forest floor biomass available to burn in grid cell *g* and year *t*, which is determined as a function of fuel moisture. $DBH_{g,t}$ is the DBH of the cohort in grid cell *g* and year *t*, which is assumed to be 40 cm if the DBH of the cohort is larger than 40 cm.

2.2.9. Cohort mortality

Mortality of trees, whether due to fire, density independent mortality, drought, or myriad other factors, is a key window of opportunity for ecological reorganization in temperate and boreal forests. Mortality events can break legacy locks associated with the dominance of long-lived trees, sometimes fostering shifts to alternate vegetation types that better match current abiotic conditions (Johnstone et al., 2016). Thus, we implemented a probabilistic and process-based approach to cohort mortality in DYNAFFOREST where trees can die from three causes: (1) fire, (2) density independent mortality, and (3) drought stress (implicitly representing death directly from hydraulic failure or increased vulnerability to biotic disturbance).

Cohort mortality from fire is determined as:

$$Pmort_{g,t} = \frac{1}{1 + e^{-1.466 + 1.91 * bt - 0.1775 * bt^2 - 5.41 * ck_{g,t}^2}} \quad \text{Eq .5}$$

where $Pmort_{g,t}$ is the probability of cohort mortality from fire in burned grid cell *g* and year *t*, *bt* is bark thickness, calculated from DBH and a PFT-specific bark thickness coefficient, and $CK_{g,t}$ is percent crown kill (Eq. (4)). This is a commonly used equation in process-based models (Hansen et al., 2020; Schumacher et al., 2006; Seidl et al., 2014).

DYNAFFOREST is capable of representing a range of fire severities, from low-severity surface fire, to stand-replacing crown fire, in each 1-km grid cell. However, it cannot simulate mixed severity fire within a grid cell. The model also currently assumes that all fires combust vegetation (section 2.2.5) and does not represent smoldering fires.

Density independent mortality is probabilistically represented following Seidl et al. (2012a) where the chances of a cohort dying increases with their age/size (Fig. 1C).

$$DIM_{g,t} = 1 - Pl^{\left(\frac{1}{Age_{max}}\right)} \quad \text{Eq. 6}$$

where $DIM_{g,t}$ is the probability of density independent mortality in cell g and year t, Pl, is the PFT-specific probability that a tree survives to its maximum age; Age_{max}, the maximum age a PFT commonly reaches in the field. Probability of cohort mortality also increases with soil drying, represented in the model as growing-season soil water potential in the rooting zone (0–100 cm soil depth), relative to average soil moisture conditions, and PFT-specific hydraulic safety margins (i.e., difference between minimum xylem water potential typically experienced in the field and the xylem water potential at which trees experience a 50% loss in conductivity) (Meinzer et al., 2009).

$$SWM_{g,t} = \frac{1}{1 + e^{-\left(a^*\left(PSI\_AVE_{g,t} - \left(PSI_{50,\,g} - \frac{HSM}{b}\right)\right)\right)}} \quad \text{Eq.7}$$

where $SWM_{g,t}$ is this year's probability of stress due to low soil moisture in cell g and year t, $PSI\_AVE_{g,t}$ is the mean growing season soil water potential in grid cell g and year t, HSM is the PFT-specific hydraulic safety margin. a and b are empirical parameters.

$PSI_{50,g}$ is median average growing season soil water potential between 2000 and 2019 in grid cell g, the period in which hydraulic safety margins were calculated in the dataset used to parameterize the model.

2.3. Model evaluation

2.3.1. Study regions

We evaluated DYNAFFOREST by simulating forests and fires in the western US forced with mid-20th century climate. We chose the western US because forest fire has long been a prevalent disturbance, and climate change is causing fire activity to rapidly increase, threatening people and ecosystems (Westerling, 2016). The western US is also data rich. For example, the USDA Forest Inventory and Analysis (FIA) network (Bechtold and Patterson, 2005) (Appendix S1) includes approximately 160,000 permanent plots across the United States designed to provide insights into forest condition. This allowed us to develop a robust parameterization for PFTs in the western US. The wealth of data also ensured that we started simulations from relatively high-quality initial conditions (described in section 2.3.2), and that we could benchmark model runs against several independent datasets (described in section 2.3.3). Parameters for the western US are provided in Appendix 2 (Tables S1 and S2).

We selected five study regions that collectively include 56% of all forested area in the western US: the coastal and Inland Pacific Northwest of Oregon and Washington (~148,000 km^2 of forest) (hereafter, PNW), northern Idaho (~97,000 km^2 of forest) (Idaho), the Greater Yellowstone Ecosystem in southern Montana and northern Wyoming (~47,500 km^2 of forest) (GYE), the southern Rockies, including parts of Utah, Colorado, New Mexico, and Arizona (~135,000 km^2 of forest) (Southern Rockies), and the Sierra Nevada Mountains (~77,000 km^2 of forest) (Sierras) (Fig. 2). Study regions were selected because they represent the range of forest types and fire regimes that characterize the western US, from dry pinyon- and ponderosa-pine woodlands, where frequent low-severity fires burned every 5–15 years prior to Euro-American settlement, to wet Douglas-fir forests of the Pacific Northwest, where fire return intervals could exceed 700 years, with infrequent yet extensive high severity, stand replacing fire events. We grouped tree species in the western US into 12 PFTs following Buotte et al. (2018) and Ruefenacht et al. (2008) (Fig. 2, Appendix S1; Table S1) and also included a grassland PFT.

2.3.2. Simulation design

We initialized the model with the gridded PFT map from Buotte et al. (2018), a stand-age map derived from remote sensing, historical fire records, and forest inventory plots (Pan et al., 2011), and information on fuel loads based on forest type (Prichard et al., 2019). Initial cohort heights were derived from the stand-age map using internal model equations (Appendix S1) (Fig. 1B). Initial DBHs, live biomass, and stand densities were calculated from initial cohort heights.

The forest ecosystem module was forced with 1965–1994 daily temperature from the TopoWx dataset (Oyler et al., 2015) and average growing season volumetric soil moisture in the rooting zone (0- to 100-cm depth), which was calculated following methods from Williams et al. (2017). Temperature data was used to calculate tree-seedling germination and establishment thresholds (section 2.2.2). Volumetric

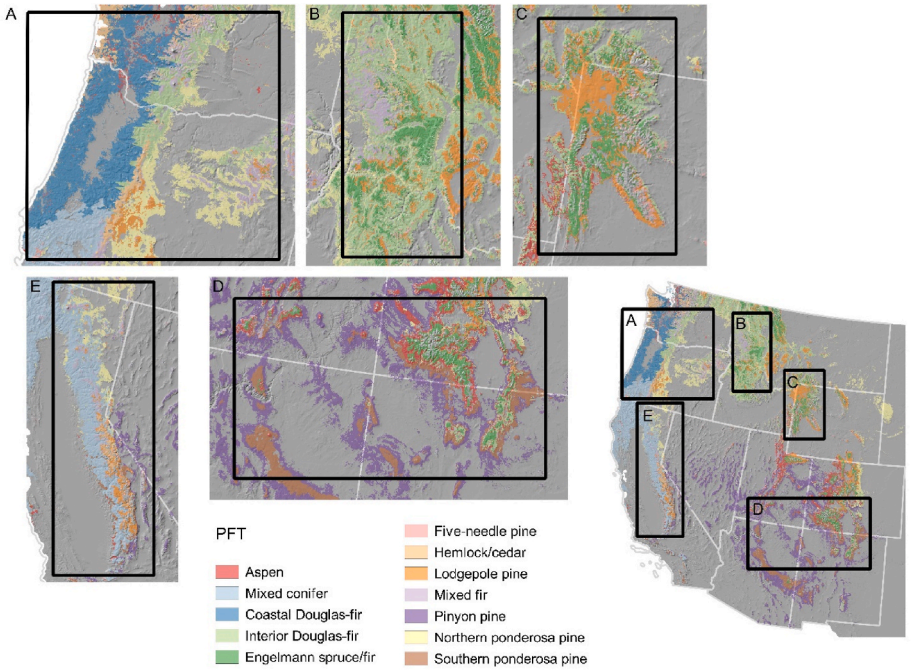

Fig. 2. (A) Pacific Northwest (PNW), (B) Idaho, (C) Greater Yellowstone Ecosystem (GYE), (D) Southern Rockies, and (E) Sierras study regions in the western United States that were simulated by DYNAFFOREST in the benchmarking experiment.

soil moisture was used in fire severity equations (section 2.2.8) and was also converted to soil water potential based on % sand, silt, and clay from SoilGrids250m 2.0 (Hengl et al., 2017) for calculations of tree regeneration (Section 2.2.2) and cohort mortality (section 2.2.9). Inputs to the fire module included the 1984–2019 climatological mean annual aridity (the ratio of total annual precipitation to total annual potential evapotranspiration) (Williams et al., 2020), topography (slope angle and topographic complexity) (Hastings and Dubar, 1999), and factors that influence fire ignition density (the 1987–2019 mean lightning strike density and 1990 human population density) (Cummins et al., 1998; Radeloff et al., 2018) (Table S3).

Initial fuel loads were representative of the forest types found in our study regions but did not reflect spatial heterogeneity due to the past legacies of harvest, fire, or drought (Prichard et al., 2019). Thus, we ran a 200-year spin up simulating the coupled response of vegetation to fire and climate in the five study regions to generate spatially heterogeneous fuels conditions consistent with internal model logic following Hansen et al. (2020). After the spin up, we ran a 100-year experiment to benchmark model performance. Because several processes are probabilistic in the model, including fire, mortality and recruitment, we ran five replicates of each region to account for model-based variability. No forest harvest was simulated.

2.3.3. Analyses – expected patterns

We benchmarked simulated forest characteristics from model year 300 and simulated fire activity from simulation years 201–300. Classical tests of statistical significance are problematic with simulated data because large sample sizes can artificially inflate significance. Thus, we used a pattern-oriented modeling approach (Grimm et al., 2005). Patterns of several simulated variables at stand (1-km grid-cell) to western-US scales were compared to observed datasets to evaluate model skill. We compared modeled and observed distributions of tree sizes and cohort densities for each PFT and region, and biomass pools and fire-regime characteristics for each region and across the western US (pooling all five study regions). Data limitations constrained our ability to benchmark the model with completely independent observational datasets, but we prioritized independence whenever possible (Table 2).

We represented model distributions of variables by calculating their median, inter-quartile range (IQR), skewness, and minimum and maximum for each PFT (when appropriate), study region, and pooling across all study regions for each of the five replicates. We then calculated the average median, IQR, skewness, and minimum, and maximum values across the replicates to compare with observed distributions. Observed distributions of tree sizes, stand densities, and biomass pools came from FIA plots that were classified as forested lands and sampled since 2000, when the USFS adopted a standard fixed-radius plot design (Bechtold and Patterson, 2005). FIA plots were not filtered based on disturbance history. For tree sizes and stand densities, model evaluation was conducted with the one-third of FIA plots that were not used in model parameterization (Appendix S1). We identified all FIA plots dominated by the PFTs represented in DYNAFFOREST and calculated the median tree height and DBH for each plot (see Appendix S1 for further details). We then compared simulated distributions of heights and DBHs with the FIA plots dominated by the same PFT. To ensure accurate comparison, we limited our analysis to simulated cohorts with a DBH >2.54 cm (the cutoff for tree measurement in FIA protocols). Observed distributions of biomass pools came from the most recent sampling of the FIA plots that were classified as forested lands, estimated using the rFIA package (Stanke et al., 2020). Because live and downed biomass routines in the forest-ecosystem module were parameterized independently from FIA (Appendix S1), we used all available FIA plots in benchmarking biomass.

Simulated annual median fire size, annual number of fires, fire perimeter shape complexity (perimeter length to patch area ratio), and annual total area burned were compared to observed fire records from the period 1985–1994 from the same database used in model parameterization (see Appendix S1). Fires came from the Western US MTBS-Interagency (WUMI) wildfire database (Juang et al., 2022), which includes large fires (>404 ha) from the US Forest Service's Monitoring Trends in Burn Severity database as well as a quality-controlled list of mostly smaller fires >100 ha maintained by the National Wildfire Coordinating group (e.g., Keeley and Syphard, 2017; Westerling et al., 2011). Because we wanted to test the fire module's ability to generate fire characteristics consistent with the mid-20th century fire regime, we chose 1985–1994 to exclude more recent observations during years where climate change has profoundly altered fire activity in the western US (Abatzoglou and Williams, 2016; Westerling, 2016). This temporal window is best suited for our current purposes because of 1) the broad spatial extent of our modeling that captures tremendous variability in fuels, aridity/climate, ignition patterns, and fire regime characteristics; and 2) because our goal in this paper was to develop a model that could generate fire consistent with mid-20th century fire seasons. Subsequent development of the fire module for forecasting interannual effects of climate on fire will require more advanced statistical models and benchmarking methods.

The simulated percent of area that burned at high severity each year was independently benchmarked against a remotely-sensed burn severity product (Parks and Abatzoglou, 2020). The database provides composite burn index (CBI) for all fires >404 ha in the observational record at a 30-m spatial resolution. To ensure the remotely-sensed product was comparable to model outputs, we first included only portions of 1985–1994 fires that fell within our initial simulated forested areas. We then masked out portions of those fires where the prefire NDVI was below 0.35 to exclude non-forested vegetation potentially misclassified as forest (Parks and Abatzoglou, 2020). We aggregated the 30-m CBI estimates within each observed fire to a 1-km^2 resolution. We used a CBI value of 2.25, equivalent to >95% tree mortality (Miller et al., 2009), as the cutoff to define stand replacing fire in each grid cell. We then calculated the percent of annual burned area that was stand replacing for each region.

We report results comparing the distributions of simulated and observed variables in three ways. To evaluate how well DYNAFFOREST captures the central tendency of each variable's observed distribution, we compared the median value and IQR from observations to the averaged median value and IQR from the simulation replicates at the PFT and/or regional, and western-US scales. To compare modeled and observed distributional shapes, we compared the skewness of variable distributions. To determine how well DYNAFFOREST represents the observed variability in each variable, we quantified what percent of observations fell between the averaged minimum and maximum values from the simulation replicates. While we assessed model skill based on

Table 2
Summary of model variables compared to observations, the benchmark datasets used, and information on whether benchmark data was independent from data used to parameterize the model.

Variable	Benchmark	Independent from parameterization?	Benchmarking Source
Tree height and DBH	USDA FIA network	Yes, 1/3 of FIA plots reserved for benchmarking	Bechtold and Patterson, 2005
Stand density	USDA FIA network	Yes, 1/3 of FIA plots reserved for benchmarking	Bechtold and Patterson, 2005
Live tree and dead forest floor biomass	USDA FIA network	Yes	Bechtold and Patterson, 2005
Number of fires, fire size, shape complexity, area burned	MTBS	No	https://www.mtbs.gov
Percent stand replacing	Reprocessed MTBS fires	Yes	Parks and Abatzoglou, 2020

the ability of DYNAFFOREST to accurately recreate observed distributions, we recognize many other factors not included in our model affect real-world forests, such as bark beetle outbreaks, forest restoration, and timber harvest (Berner et al., 2017). Thus, we anticipated that these unaccounted for drivers of forest dynamics would generate some divergence between simulated and observed central tendencies, distributional shapes, and ranges of variability.

Benchmarking analyses were conducted in R statistical software V. 4.0.4 (Core Team, 2021) using the packages rFIA (Stanke et al., 2020), tidyverse (Wickham et al., 2019), ncdf4 (Pierce, 2017), landscapemetrics (Hesselbarth et al., 2019), sf (Pebesma, 2018), dbplyr (Wickham and Ruiz, 2020), moments (Lukasz and Novomestky, 2015), and raster (Hijmans, 2021). Simulations and processing of model outputs were run on the Amarel cluster at Rutgers University.

3. Results

3.1. Tree size, stand density, and forest cover

Among PFTs, modeled median tree heights and DBHs differed from observations of the same PFT by 16% and 20%, on average. Averaged across PFTs, the skew of modeled and observed tree heights was −1.3 and 1.2, and the skew of modeled and observed DBHs was −1.3 and 2.0 (Table 3). Model skill in representing tree heights and DBHs varied across PFTs (Fig. 3). For example, simulated aspen trees were shorter, on average, and had smaller diameters than observed aspen, while modeled inland Douglas-fir tended to be larger than observations. DYNAFFOREST captured much of the variability in observed tree heights and DBHs, however. On average, 68% of observations fell within the ranges of simulated tree heights and DBHs of the same PFT. Some variability also existed between regions in how well the model captured observed median tree sizes (Figs. S1 and S2). For example, modeled median heights of mixed firs closely matched the observed medians in Idaho, PNW, and Sierras, but aspen trees in DYNAFFOREST were considerably taller than observations in the Southern Rockies (Fig. S1).

Modeled median stand density was within 39% of the observed median stand density of the same PFT, on average. The skew of modeled and observed stand densities was 4.3 and 4.8 (Table 3). The median simulated stands of Engelmann spruce/fir, hemlock/cedar, five needle pine, and lodgepole pine were moderately denser than observations, while the median simulated stands of mixed conifer, coastal Douglas-fir, and inland Douglas-fir were less dense (Fig. 4). An average of 62% of observations fell within the range of simulated stand densities of the same PFT. Model skill also varied among regions (Fig. S3). Median inland Douglas-fir densities in the model, for example, were lower than observed medians in the GYE, Idaho, PNW and Southern Rockies, but were higher than observed in the Sierras (Fig. S3).

Eight percent of initial forest area converted to grassland by simulation year 300, on average across the five study regions. The grassland PFT was most common in the Sierras, where it replaced 15% of initial forest area, followed by the PNW (9%), Southern Rockies (8%), GYE (5%), and was least common in Idaho, where it replaced 4% of forest area after 300 years of simulation. Expansion of grassland was unsurprising, as the PFT distributions used to initialize simulations did not include grassland, and it is often interspersed within western forest ecosystems.

3.2. Biomass pools

Pooling all study regions together, there was strong model-observation correspondence in live biomass; the average median leaf and aboveground live wood biomass from the five simulation replicates were within 29% and 12% of the observed medians, respectively (Table 3, Fig. 5A). The skew of modeled and observed leaf biomass was 1.4 and 2.2, and the skew of modeled and observed aboveground live wood biomass was 1.1 and 2.3 (Table 3). The model also represented observed variability in live biomass well. Across all study regions, 90% and 92% of observations fell within the range of simulations for leaf and aboveground woody biomass. Median live aboveground tree biomass was highest in the Idaho study region, followed closely by the PNW, GYE, Sierras, and Southern Rockies (Table S4. Fig. 6). When model outputs were compared with observations within regions, median leaf biomass was underestimated by DYNAFFOREST in the PNW and was overestimated in the other study regions (Table S4). Modeled median live aboveground woody biomass was lower than observations in the PNW and Sierras and was higher in the Southern Rockies, Idaho, and GYE.

Average median litter and coarse wood biomass were within 5% and 7%, of the median observed values, respectively (Fig. 5B). The skew of modeled and observed litter biomass was 1.7 and 5.3, and the skew of modeled and observed aboveground coarse wood biomass was 2.5 and 3.4 (Table 3). Across all study regions, 98% and 100% of observations fell within the range of simulations for downed litter and coarse wood pools, suggesting the model could reasonably represent the range of variability in downed biomass. However, variability did exist in model-observation correspondence when broken out by study region (Table S1, Fig. S4). DYNAFFOREST underestimated median litter biomass in the Sierras and PNW and overestimated median litter biomass in the other regions. Modeled median coarse wood biomass was also lower than in the observational dataset in the PNW, Idaho, and GYE, and larger than

Table 3
Median modeled and observed biomass and fire characteristics across the western US. Modeled biomass and fire characteristics values are averaged from five simulation replicates.

	Model				Observations			
	Median	25th %ile	75th %ile	Skew	Median	25th %ile	75th %ile	Skew
Tree size and density								
DBH (cm)	29.1	19.0	35.4	−1.3	23.8	18.4	35.1	2.0
Height (m)	15.7	10.5	19.0	−1.3	14.8	10.8	20.3	1.2
Density (stems ha^{-1})	407	364	736	4.3	441	244	717	4.8
Live biomass								
Leaf (kg ha^{-1})	5,599	4,008	6,593	1.4	4,163	1,297	9,263	2.2
Woody aboveground (kg ha^{-1})	75,272	30,655	116,438	1.1	67,021	20,475	155,960	2.3
Downed biomass								
Litter (kg ha^{-1})	5,869	4,257	6,914	1.7	6,153	2,844	11,515	5.3
Coarse wood (kg ha^{-1})	13,347	9,771	22,648	2.5	12,471	3,656	28,809	3.4
Fire characteristics								
Number of fires	59.3	54.75	65.1	0.2	62	49.5	96	1.0
Perimeter:area (m ha^{-1})	24	24	26	1.9	30	29	30	1.3
Fire size (ha)	500	400	500	−0.8	200	200	300	−0.5
Area burned (ha)	36,160	29,800	44,945	1.0	62,500	28,450	128,250	1.9
percent area burned as stand replacing (%)	17.4	10.9	21.6	2.1	12.8	5.5	27.8	0.9

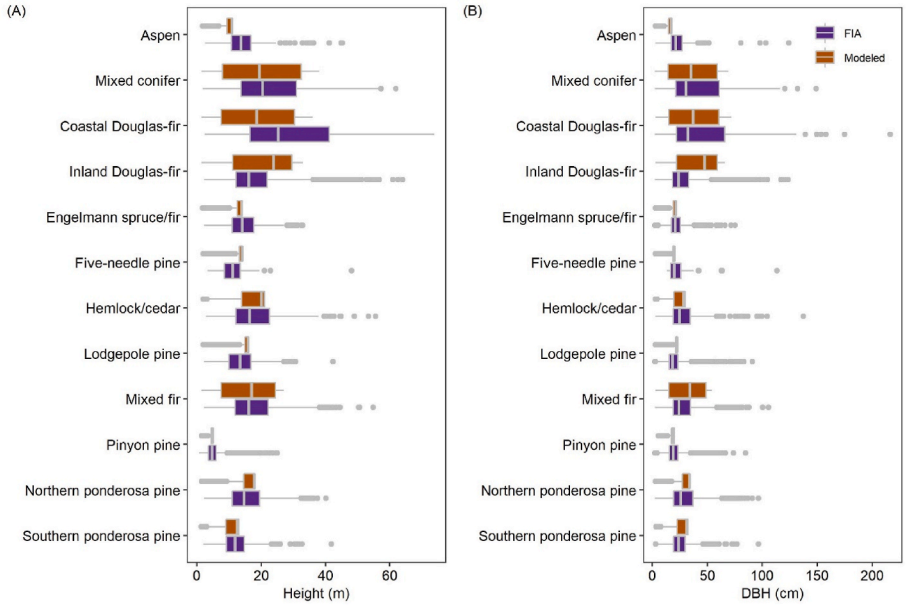

Fig. 3. Observed and modeled (A) tree heights and (B) diameter at 1.35m (DBH) for 12 PFTs across five large regions of the western United States. Observations were derived from US Forest Service Forest Inventory and Analysis (FIA) plots independent from those used in parameterization. Simulated tree DBHs came from simulation year 300 of replicate run 1 and excluded trees with DBH <2.54 cm to match observations. Observed sample size = 11,182. Modeled sampled size = 419,189.

observed in the Sierras and Southern Rockies.

3.3. Fire-regime characteristics

Pooling all study regions together, the annual median number of fires, fire size, perimeter to area ratio, annual area burned, and percent of annual burned area that was stand replacing from simulations differed from observed medians by 4%, 86%, 22%, 53%, and 31%, respectively (Table 3, Fig. 7). DYNAFFOREST overestimated the annual median fire size but also did not simulate rare extremely large observed fire years, such as the 1988 Yellowstone fires (Fig. S5), which caused the model to underestimate median annual area burned (Fig. 7B), and may have contributed to the model's over-representation of live biomass in the GYE (Fig. 6). Approximately half of observations fell within the range of simulations for the annual number of fires and area burned. While only 36% of observations fell within the range of simulations for annual median fire size, 82% and 98% of observations fell within the range of simulations for the perimeter to area ratio and the percent of annual burned area that was stand replacing, respectively. Substantial variability in model-observation correspondence existed when evaluating the fire module within study regions (Table S4, Fig. S5). For example, annual area burned was most strongly underestimated by the model in the GYE, where the iconic 1988 Yellowstone fires took place, reinforcing the importance of rare extremely large fire years for shaping model-observation disparities in fire characteristics.

4. Discussion

Fires and forests dynamically influence one another through disturbance-succession cycles (Parks et al., 2015; Prichard et al., 2017). Where, when, and why fire-induced changes to temperate and boreal forests may feedback to affect subsequent burning remains poorly resolved, particularly at regional to continental scales (Abatzoglou et al., 2021; Hurteau et al., 2019). Here, we present a new approach to address this challenge. DYNAFFOREST combines a hybrid probabilistic and deterministic process-based forest-ecosystem module with a flexible statistical fire module. Benchmarking results demonstrate that the forest-ecosystem module reasonably recreates patterns of diverse forest characteristics across broad spatial domains (~850,000 km^2 of forest in the western US). The fire module as currently conceptualized captures average 20th-century fire characteristics in five study regions with highly variable fire regimes. However, the fire module misses the extremely large fire events that were relatively rare over the last century because we did not include effects of temporal climate variability on fire occurrence and size in this first version. Our baseline model provides proof of concept and will continue to be refined and expanded to meet the need for bottom-up forest and fire projections that can inform forest management and adaptation strategies (Filotas et al., 2014; Messier et al., 2015). For example, DYNAFFOREST could be used in the future to evaluate where, when, and at what spatial scales different combinations of thinning and prescribed fire could decouple 21st-century climate-fire relationships.

A key objective of the forest-ecosystem module was to explicitly include the demographic processes through which climate and fire affect forests and initiate feedbacks that can influence subsequent fire. We accomplished this in a computationally efficient manner by taking a probabilistic approach for representing a few key processes, such as seed dispersal, seedling establishment, and tree mortality, while deterministically representing others based on successional stage. The model generated patterns of forest cover and structure consistent with observations across five diverse study regions. Importantly, the model also captured examples of type conversions. The PFT maps used to initialize simulations did not include grassland, even though it is commonly interspersed among some forests of the western US. However, simulated forests that experienced low soil moisture and/or unusually frequent and large high severity fires converted to nonforest in all study regions, generating realistic forest-grassland mosaics at low elevations in the Sierras and Southern Rockies study regions and in southern and eastern Oregon (part of the PNW study region). Such patterns are consistent with recent analyses of drought-induced forest conversion (Davis et al., 2019), and highlight how DYNAFFOREST could be a powerful tool for quantifying 21st-century forest resilience and transformation by identifying the climate-fire tipping points that initiate wide spread conversion to grassland (Coop et al., 2020; Hansen et al., 2020; Hansen and Turner, 2019).

We set out to generate a parameter set for the forest-ecosystem module that was robust across all of the western US, and DYNAFFOREST was particularly skilled at capturing patterns of forest structure when outputs from the five study regions were pooled to the western-US scale. However, variation in model-observation correspondence within study regions highlights inevitable tradeoffs between maximizing model realism and distilling immense ecological complexity into a tractable

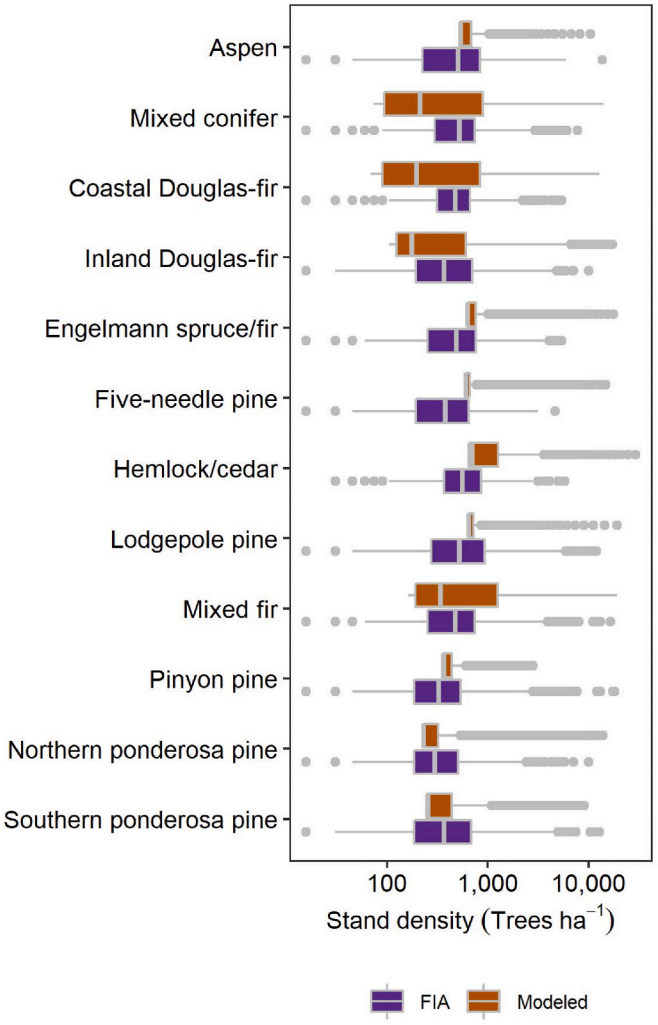

Fig. 4. Observed and modeled stand density for 12 PFTs across five large regions of the western United States. Observations were derived from US Forest Service Forest Inventory and Analysis plots independent from those used in parameterization. Simulated stand densities came from simulation year 300 of replicate run 1 and excluded trees with DBH <2.54 cm to match observations. Observed sample size = 18,306. Modeled sampled size = 419,189.

system representation. For example, tree size and stand density were deterministic in DYNAFFOREST, based solely on the previous year's state. This means that myriad abiotic and biotic factors such as climate, nutrient availability, and interspecific competition were not explicitly considered. Thus, we expected DYNAFFOREST to overestimate tree growth and stand density on the trailing and leading edges of PFT ranges where environmental conditions are harsh (arid/cold). Indeed, the model did not capture the lowest density stands observed for most PFTs

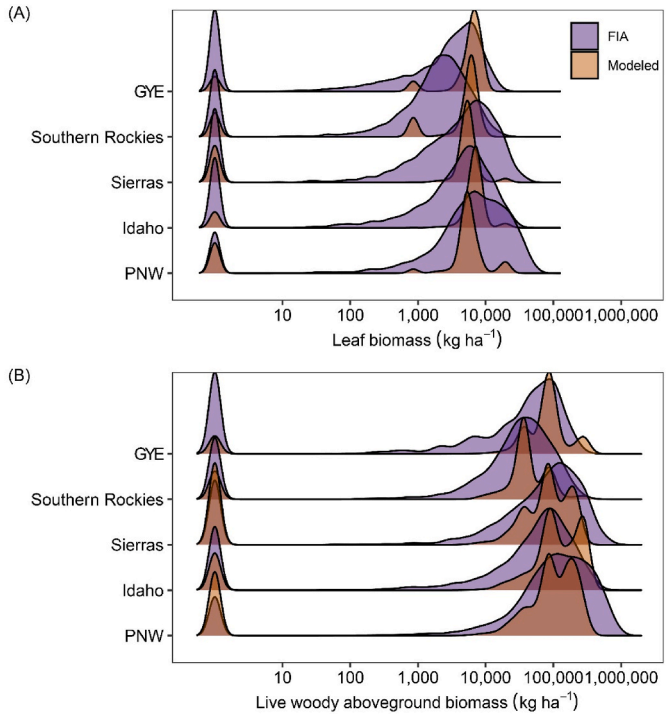

Fig. 6. Distributions of observed and simulated (A) leaf and (B) woody aboveground live biomass in five large study regions of the western United States. Observations were derived from US Forest Service Forest Inventory and Analysis plots classified as forested lands. Simulated total aboveground live tree biomass came from year 300 simulation replicate 1. The multi-modal distributions of simulated biomass are due to the discrete representation of forest communities as a few PFTs. Low biomass peaks in simulations are recently burned stands that experienced stand replacing fire. Low biomass peaks in observations occur because observations were not filtered by disturbance history.

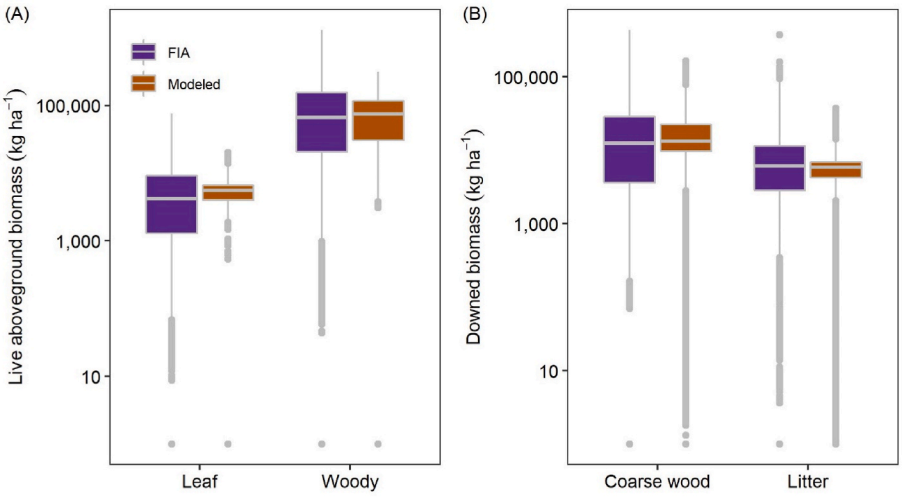

Fig. 5. Distributions of observed and simulated (A) leaf, and aboveground woody live biomass, and (B) downed coarse wood and litter biomass across five regions of the western United States. Observations were derived from US Forest Service Forest Inventory and Analysis plots independent from those used in parameterization. Simulated total aboveground live tree biomass came from year 300 of replicate run 1. Observed sample size = 23,364. Modeled sampled size = 503,765 for live biomass variables. Observed sample size = 20,288. Modeled sampled size = 503,765 for downed biomass variables.

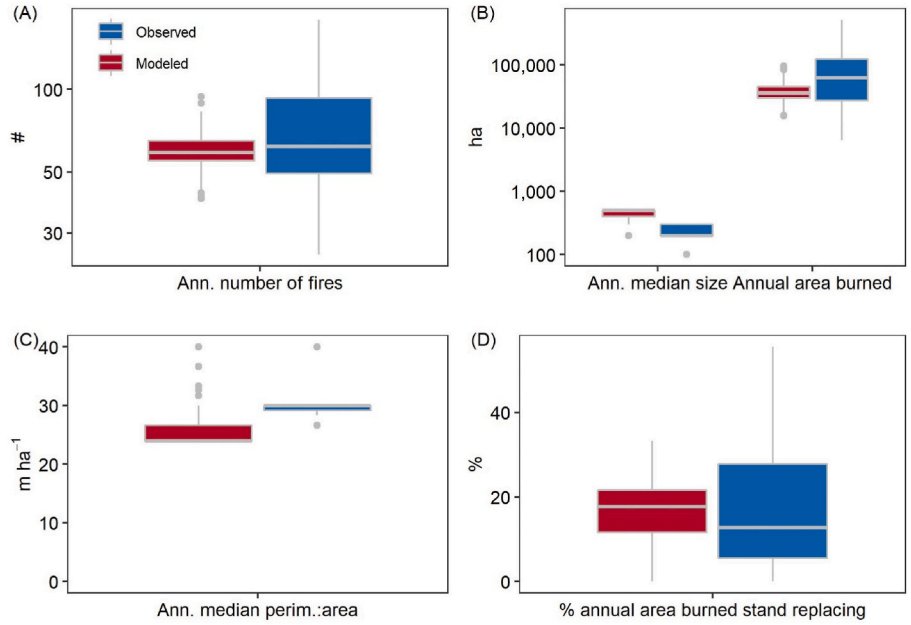

Fig. 7. Distributions of observed and simulated (A) annual number of fires, (B) annual median fire size and total annual area burned, (C) annual median perimeter length to patch area ratio, and (D) percent of annual burned area that was stand replacing across five regions of the western United States. Observations were for fires between 1985 and 1994. Simulated fires were from years 201–300 of replicate run 1.

(Fig. 4). This may explain some of the variability in model-observation correspondence between study regions as well as any mismatch between simulated and observed distribution shapes (as quantified by skewness) of PFT tree size and stand density, even when there was agreement for medians and IQRs of distributions. Trait values also vary tremendously across PFT ranges (Anderegg et al., 2018; Messier et al., 2010, 2017), and regional variability in model performance highlights how PFT parameterizations must be tailored to the scale at which questions are being asked.

DYNAFFOREST includes a flexible statistical fire module that can be adapted to meet the needs of many different applications. Here, we implemented a relatively simple representation where fire occurrence and size were only sensitive to forest biomass and spatial variability in mean aridity, lightning frequency, topography, and human population, but did not respond to inter-annual variability in climate or within-season extreme fire weather. This explains why the model was modestly skilled at capturing the average characteristics of 20th-century forest fires but did not simulate as much inter-annual variability in fire activity as observed. In reality, inter-annual variability of atmospheric aridity is a dominant driver of burned area in temperate and boreal forests (Abatzoglou and Williams, 2016; Higuera and Abatzoglou, 2020; Seidl et al., 2020). An essential next step in the development of DYNAFFOREST is to represent how temporal changes in climate affect fire occurrence and size.

Even now, however, DYNAFFOREST includes far more realism in its representation of fire than many other models operating at this scale. For example, of nine ESMs evaluated in the Fire Inter-Model Comparison Project, nearly half prescribed vegetation rather than dynamically coupling fire and forests; only one-third explicitly simulated individual fires instead of aggregate burned area; and all operated at coarse spatial resolutions ($\geq 0.5^{\circ}$ grid cells), meaning they were incapable of representing fine-scale spatial heterogeneity within individual fire perimeters (Hantson et al., 2020; Rabin et al., 2017). In contrast, DYNAFFOREST explicitly couples fire and vegetation dynamics, simulates individual fire occurrence and size as a function of human and natural drivers, and dynamically grows individual fires at a 1-km spatial resolution based on fuel availability. The model also simulates heterogeneity of fire severity within burned perimeters. Thus, DYNAFFOREST is uniquely capable of capturing the complex finer-scale patterns generated by fires across broad spatial domains as compared with many other models.

5. Conclusions

We present a new model for simulating the dynamic interactions and feedbacks between fire and temperate and boreal forests. Our approach fills a unique need by 1) explicitly representing the key forest demographics through which fire affects forests 2) capturing the spatially heterogeneous effects of individual fires, and 3) simulating regional to continental domains for decades to centuries. Such tools are desperately needed by scientists and decision makers to determine where, when, and why fire-induced changes to forests may feedback to affect subsequent burning (McWethy et al., 2019) and affect regional forest conditions. Better constrained projections of changing fire and forests could inform policy and management strategies designed to help people more sustainably coexist with fire now and in the future (Cochrane and Bowman, 2021), to focus on important questions of forest carbon, biodiversity conservation, forest economics, and fire hazard.

Software and data availability

Software name: DYNAFFOREST (**DYNA**mic Temperate and Boreal Fire and **FOR**est-Ecosy**ST**em Simulator).
Developer: Winslow D. Hansen.
First year available: 2022.
Hardware requirements: PC/Mac.
Software requirements: R statistical environment and language.
Program language: R.
Program size: 121.5 kb.
Availability: http://forestfutureslab.org/dynafforest
License: GPL-3.0.
Archive with data from benchmarking: Data archive can be found at: 10.25390/caryinstitute.20452386.
Size of archive: 157 MB

Author contributions

WDH developed the model with input from APW, WDH conducted the benchmarking exercises with input from all coauthors, WDH wrote the paper and all coauthors contributed to revisions.

Declaration of competing interest

The authors declare that they have no known competing financial interests or personal relationships that could have appeared to influence the work reported in this paper.

Acknowledgements

WDH acknowledges support from the Gordon and Betty Moore Foundation (Grant # GBMF10763), the Royal Bank of Canada, the Environmental Defense Fund, and the National Science Foundation (Grant # OPP 2116863). APW acknowledges support from the Zegar Family Foundation and DOE grant DESC0022302. ATT acknowledges funding from the NSF Grants 2003205 and 2017949, the USDA National Institute of Food and Agriculture, Agricultural and Food Research Initiative Competitive Programme Grant No. 2018-67012-31496 and the University of California Laboratory Fees Research Program Award No. LFR-20-652467. We thank Rupert Seidl and Werner Rammer for sharing their expertise on the development of forest simulation models.

Appendix A. Supplementary data

Supplementary data to this article can be found online at https://doi.org/10.1016/j.envsoft.2022.105473.

References

Abatzoglou, J.T., Williams, A.P., 2016. Impact of anthropogenic climate change on wildfire across western US forests. Proc. Natl. Acad. Sci. 113, 11770–11775. https://doi.org/10.1073/pnas.1607171113.

Abatzoglou, J.T., Battisti, D.S., Williams, A.P., Hansen, W.D., Harvey, B.J., Kolden, C.A., 2021. Projected increases in western US forest fire despite growing fuel constraints. Commun. Earth Environ. 2, 1–8. https://doi.org/10.1038/s43247-021-00299-0.

Albrich, K., Rammer, W., Turner, M.G., Ratajczak, Z., Braziunas, K.H., Hansen, W.D., Seidl, R., 2020. Simulating forest resilience: a review. Global Ecol. Biogeogr. 29, 2082–2096. https://doi.org/10.1111/geb.13197.

Anderegg, L.D.L., Berner, L.T., Badgley, G., Sethi, M.L., Law, B.E., HilleRisLambers, J., 2018. Within-species patterns challenge our understanding of the leaf economics spectrum. Ecol. Lett. 21, 734–744. https://doi.org/10.1111/ele.12945.

Balch, J.K., Bradley, B.A., Abatzoglou, J.T., Nagy, R.C., Fusco, E.J., Mahood, A.L., 2017. Human-started wildfires expand the fire niche across the United States. Proc. Natl. Acad. Sci. 114, 2946–2951. https://doi.org/10.1073/pnas.1617394114.

Bechtold, W.A., Patterson, P.L., 2005. The enhanced forest inventory and analysis program-national sampling design and estimation procedures (No. General technical report SRS–80). In: Southern Research Station. USDA Forest Service, Asheville, NC, USA.

Becknell, J.M., Desai, A.R., Dietze, M.C., Schultz, C.A., Starr, G., Duffy, P.A., Franklin, J. F., Pourmokhtarian, A., Hall, J., Stoy, P.C., Binford, M.W., Boring, L.R., Staudhammer, C.L., 2015. Assessing interactions among changing climate, management, and disturbance in forests: a macrosystems approach. Bioscience 65, 263–274. https://doi.org/10.1093/biosci/biu234.

Berner, L.T., Law, B.E., Meddens, A.J.H., Hicke, J.A., 2017. Tree mortality from fires, bark beetles, and timber harvest during a hot and dry decade in the western United States (2003–2012). Environ. Res. Lett. 12, 065005 https://doi.org/10.1088/1748-9326/aa6f94.

Braziunas, K.H., Hansen, W.D., Seidl, R., Rammer, W., Turner, M.G., 2018. Looking beyond the mean: drivers of variability in postfire stand development of conifers in Greater Yellowstone. For. Ecol. Manag. 430, 460–471. https://doi.org/10.1016/j.foreco.2018.08.034.

Brown, C.D., Dufour-Tremblay, G., Jameson, R.G., Mamet, S.D., Trant, A.J., Walker, X.J., Boudreau, S., Harper, K.A., Henry, G.H.R., Hermanutz, L., Hofgaard, A., Isaeva, L., Kershaw, G.P., Johnstone, J.F., 2019. Reproduction as a bottleneck to treeline advance across the circumarctic forest tundra ecotone. Ecography 42, 137–147. https://doi.org/10.1111/ecog.03733.

Brown, C.D., Johnstone, J.F., 2012. Once burned, twice shy: Repeat fires reduce seed availability and alter substrate constraints on Picea mariana regeneration. For. Ecol. Manag. 266, 34–41. https://doi.org/10.1016/j.foreco.2011.11.006.

Buma, B., Brown, C.D., Donato, D.C., Fountain, J.B., Johnstone, J.F., 2013. The impacts of changing disturbance regimes on serotinous plant populations and communities. BioScience 63 (11), 866–876. https://doi.org/10.1525/bio.2013.63.11.5.

Buotte, P.C., Levis, S., Law, B.E., Hudiburg, T.W., Rupp, D.E., Kent, J.J., 2018. Near-future forest vulnerability to drought and fire varies across the western United States. Global Change Biol. 25, 290–303. https://doi.org/10.1111/gcb.14490.

Burton, P.J., Cumming, S.G., 1995. Potential effects of climatic change on some western Canadian forests, based on phenological enhancements to a patch model of forest succession. Water, Air, Soil Pollut. 82, 401–414. https://doi.org/10.1007/BF01182850.

Calef, M.P., McGuire, A.D., Chapin III, F.S., 2008. Human influences on wildfire in Alaska from 1988 through 2005: an analysis of the spatial patterns of human impacts. Earth Interact. 12, 1–17.

Cochrane, M.A., Bowman, D.M.J.S., 2021. Manage fire regimes, not fires. Nat. Geosci. 14, 455–457. https://doi.org/10.1038/s41561-021-00791-4.

Coop, J.D., Parks, S.A., Stevens-Rumann, C.S., Crausbay, S.D., Higuera, P.E., Hurteau, M. D., Tepley, A., Whitman, E., Assal, T., Collins, B.M., Davis, K.T., Dobrowski, S., Falk, D.A., Fornwalt, P.J., Fulé, P.Z., Harvey, B.J., Kane, V.R., Littlefield, C.E., Margolis, E.Q., North, M., Parisien, M.-A., Prichard, S., Rodman, K.C., 2020. Wildfire-driven forest conversion in western North American landscapes. Bioscience 70, 659–673. https://doi.org/10.1093/biosci/biaa061.

Core Team, R., 2021. R: A Language and Environment for Statistical Computing.

Cummins, K.L., Krider, E.P., Malone, M.D., 1998. The US National Lightning Detection Network/sup TM/and applications of cloud-to-ground lightning data by electric power utilities. IEEE Trans. Electromagn C. 40, 465–480. https://doi.org/10.1109/15.736207.

Davis, K.T., Dobrowski, S.Z., Higuera, P.E., Holden, Z.A., Veblen, T.T., Rother, M.T., Parks, S.A., Sala, A., Maneta, M.P., 2019. Wildfires and climate change push low-elevation forests across a critical climate threshold for tree regeneration. Proc. Natl. Acad. Sci. 116, 6193–6198. https://doi.org/10.1073/pnas.1815107116.

Dixon, G.E., 2015. Essential FVS : A User's Guide to the Forest Vegetation Simulator. United States Department of Agriculture, Forest Management Service Center, Forth Collins, CO.

Filotas, E., Parrott, L., Burton, P.J., Chazdon, R.L., Coates, K.D., Coll, L., Hauesser, S., Martin, K., Nocentini, S., Puettmann, K.J., Putz, F.E., Simard, S.W., Messier, C., 2014. Viewing forests through the lens of complex systems science. Ecosphere 5, 1–23.

Fisher, R.A., Koven, C.D., Anderegg, W.R.L., Christoffersen, B.O., Dietze, M.C., Farrior, C. E., Holm, J.A., Hurtt, G.C., Knox, R.G., Lawrence, P.J., Lichstein, J.W., Longo, M., Matheny, A.M., Medvigy, D., Muller-Landau, H.C., Powell, T.L., Serbin, S.P., Sato, H., Shuman, J.K., Smith, B., Trugman, A.T., Viskari, T., Verbeeck, H., Weng, E., Xu, C., Xu, X., Zhang, T., Moorcroft, P.R., 2018. Vegetation demographics in Earth System Models: a review of progress and priorities. Global Change Biol. 24, 35–54. https://doi.org/10.1111/gcb.13910.

Gill, N.S., Turner, M.G., Brown, C.D., Glassman, S.I., Haire, S.L., Hansen, W.D., Pansing, E.R., St Clair, S.B., Tomback, D.F., 2022. Limitations to propagule dispersal will constrain postfire recovery of plants and fungi in western coniferous forests. BioScience biab139. https://doi.org/10.1093/biosci/biab139.

Grimm, V., Revilla, E., Berger, U., Jeltsch, F., Mooij, W.M., Railsback, S.F., Thulke, H.-H., Weiner, J., Wiegand, T., DeAngelis, D.L., 2005. Pattern-oriented modeling of agent-based complex systems: lessons from ecology. Science 310, 987–991. https://doi.org/10.1126/science.1116681.

Hagmann, R.K., Hessburg, P.F., Prichard, S.J., Povak, N.A., Brown, P.M., Fulé, P.Z., Keane, R.E., Knapp, E.E., Lydersen, J.M., Metlen, K.L., Reilly, M.J., Sánchez Meador, A.J., Stephens, S.L., Stevens, J.T., Taylor, A.H., Yocom, L.L., Battaglia, M.A., Churchill, D.J., Daniels, L.D., Falk, D.A., Henson, P., Johnston, J.D., Krawchuk, M.A., Levine, C.R., Meigs, G.W., Merschel, A.G., North, M.P., Safford, H.D., Swetnam, T. W., Waltz, A.E.M., 2021. Evidence for widespread changes in the structure, composition, and fire regimes of western North American forests. Ecol. Appl. 31, e02431 https://doi.org/10.1002/eap.2431.

Hansen, W.D., Turner, M.G., 2019. Origins of abrupt change? Postfire subalpine conifer regeneration declines nonlinearly with warming and drying. Ecol. Monogr. 89, e01340 https://doi.org/10.1002/ecm.1340.

Hansen, W.D., Braziunas, K.H., Rammer, W., Seidl, R., Turner, M.G., 2018. It takes a few to tango: changing climate and fire regimes can cause regeneration failure of two subalpine conifers. Ecology 99, 966–977. https://doi.org/10.1002/ecy.2181.

Hansen, W.D., Abendroth, D., Rammer, W., Seidl, R., Turner, M.G., 2020. Can wildland fire management alter 21st-century subalpine fire and forests in Grand Teton National Park, Wyoming, USA? Ecol. Appl. 30, e02030 https://doi.org/10.1002/eap.2030.

Hansen, W.D., Fitzsimmons, R., Olnes, J., Williams, A.P., 2021. An alternate vegetation type proves resilient and persists for decades following forest conversion in the North American boreal biome. J. Ecol. 109, 85–98. https://doi.org/10.1111/1365-2745.13446.

Hantson, S., Kelley, D.I., Arneth, A., Harrison, S.P., Archibald, S., Bachelet, D., Forrest, M., Hickler, T., Lasslop, G., Li, F., Mangeon, S., Melton, J.R., Nieradzik, L., Rabin, S.S., Prentice, I.C., Sheehan, T., Sitch, S., Teckentrup, L., Voulgarakis, A., Yue, C., 2020. Quantitative assessment of fire and vegetation properties in simulations with fire-enabled vegetation models from the Fire Model Intercomparison Project. Geosci. Model Dev. (GMD) 13, 3299–3318. https://doi.org/10.5194/gmd-13-3299-2020.

Harvey, B.J., Donato, D.C., Turner, M.G., 2016. Drivers and trends in landscape patterns of stand-replacing fire in forests of the US Northern Rocky Mountains (1984–2010). Landsc. Ecol. 31, 2367–2383. https://doi.org/10.1007/s10980-016-0408-4.

Hastings, D.A., Dubar, P.K., 1999. Global Land One-Kilometer Base Elevation Digital Elevation Mode, Version 1.0. National Oceanic and Atmospheric Administration. National Geophysical Data Center, Boulder, CO.

Heffernan, J.B., Soranno, P.A., Angilletta, M.J., Buckley, L.B., Gruner, D.S., Keitt, T.H., Kellner, J.R., Kominoski, J.S., Rocha, A.V., Xiao, J., Harms, T.K., Goring, S.J.,

Koenig, L.E., McDowell, W.H., Powell, H., Richardson, A.D., Stow, C.A., Vargas, R., Weathers, K.C., 2014. Macrosystems ecology: understanding ecological patterns and processes at continental scales. Front. Ecol. Environ. 12, 5–14. https://doi.org/10.1890/130017.

Hengl, T., Jesus, J.M. de, Heuvelink, G.B.M., Gonzalez, M.R., Kilibarda, M., Blagotić, A., Shangguan, W., Wright, M.N., Geng, X., Bauer-Marschallinger, B., Guevara, M.A., Vargas, R., MacMillan, R.A., Batjes, N.H., Leenaars, J.G.B., Ribeiro, E., Wheeler, I., Mantel, S., Kempen, B., 2017. SoilGrids250m: global gridded soil information based on machine learning. PLoS One 12, e0169748. https://doi.org/10.1371/journal.pone.0169748.

Hesselbarth, M.H.K., Sciaini, M., With, K.A., Wiegand, K., Nowosad, J., 2019. landscapemetrics: an open-source R tool to calculate landscape metrics. Ecography 42, 1648–1657. https://doi.org/10.1111/ecog.04617.

Higuera, P.E., Abatzoglou, J.T., 2020. Record-setting climate enabled the extraordinary 2020 fire season in the western United States. Global Change Biol. 27, 1–2. https://doi.org/10.1111/gcb.15388.

Hijmans, R.J., 2021. Terra: Spatial Data Analysis.

Honkaniemi, J., Rammer, W., Seidl, R., 2021. From mycelia to mastodons – a general approach for simulating biotic disturbances in forest ecosystems. Environ. Model. Software 138, 104977. https://doi.org/10.1016/j.envsoft.2021.104977.

Hurteau, M.D., Liang, S., Westerling, A.L., Wiedinmyer, C., 2019. Vegetation-fire feedback reduces projected area burned under climate change. Sci. Rep. 9, 2838. https://doi.org/10.1038/s41598-019-39284-1, 2838.

Johnson, D.M., McCulloh, K.A., Reinhard, K., 2011. The earliest stages of tree growth: development, physiology and impacts of microclimate. In: Day, M.E., Greenwood, M. S. (Eds.), Size- and Age-Related Changes in Tree Structure and Function, pp. 91–119. https://doi.org/10.1007/978-94-007-1242-3.

Johnstone, J.F., Allen, C.D., Franklin, J.F., Frelich, L.E., Harvey, B.J., Higuera, P.E., Mack, M.C., Meentemeyer, R.K., Metz, M.R., Perry, G.L., Schoennagel, T., Turner, M. G., 2016. Changing disturbance regimes, ecological memory, and forest resilience. Front. Ecol. Environ. 14, 369–378. https://doi.org/10.1002/fee.1311.

Juang, C.S., Williams, A.P., Abatzoglou, J.T., Balch, J.K., Hurteau, M.D., Moritz, M.A., 2022. Rapid growth of large forest fires drives the exponential response of annual forest-fire area to aridity in the western United States. Geophys. Res. Lett. 49, e2021GL097131 https://doi.org/10.1029/2021GL097131.

Keeley, J.E., Syphard, A.D., 2017. Different historical fire–climate patterns in California. Int. J. Wildland Fire 26, 253–268. https://doi.org/10.1071/WF16102.

Kelly, R., Chipman, M.L., Higuera, P.E., Stefanova, I., Brubaker, L.B., Hu, F.S., 2013. Recent burning of boreal forests exceeds fire regime limits of the past 10,000 years. Proc. Natl. Acad. Sci. 110, 13055–13060. https://doi.org/10.1073/pnas.1305069110.

Keyser, A.R., Westerling, A.L., 2019. Predicting increasing high severity area burned for three forested regions in the western United States using extreme value theory. For. Ecol. Manag. 432, 694–706. https://doi.org/10.1016/J.FORECO.2018.09.027.

Kitzberger, T., Falk, D.A., Westerling, A.L., Swetnam, T.W., 2017. Direct and indirect climate controls predict heterogeneous early-mid 21st century wildfire burned area across western and boreal North America. PLoS One 12. https://doi.org/10.1371/journal.pone.0188486 e0188486–e0188486.

Kueppers, L.M., Conlisk, E., Castanha, C., Moyes, A.B., Germino, M.J., de Valpine, P., Torn, M.S., Mitton, J.B., 2017. Warming and provenance limit tree recruitment across and beyond the elevation range of subalpine forest. Global Change Biol. 23, 2383–2395. https://doi.org/10.1111/gcb.13561.

Littell, J.S., McKenzie, D., Wan, H.Y., Cushman, S.A., 2018. Climate change and future wildfire in the western United States: an ecological approach to nonstationarity. Earth's Future 6, 1097–1111. https://doi.org/10.1029/2018EF000878.

Lukasz, K., Novomestky, F., 2015. Moments: Moments, Cumulants, Skewness, Kurtosis and Related Tests. R package version 0.14.

McWethy, D.B., Schoennagel, T., Higuera, P.E., Krawchuk, M., Harvey, B.J., Metcalf, E. C., Schultz, C., Miller, C., Metcalf, A.L., Buma, B., Virapongse, A., Kulig, J.C., Stedman, R.C., Ratajczak, Z., Nelson, C.R., Kolden, C., 2019. Rethinking resilience to wildfire. Nat. Sustain. 2, 797–804. https://doi.org/10.1038/s41893-019-0353-8.

Meinzer, F.C., Johnson, D.M., Lachenbruch, B., McCulloh, K.A., Woodruff, D.R., 2009. Xylem hydraulic safety margins in woody plants: coordination of stomatal control of xylem tension with hydraulic capacitance. Funct. Ecol. 23, 922–930. https://doi.org/10.1111/j.1365-2435.2009.01577.x.

Messier, J., McGill, B.J., Lechowicz, M.J., 2010. How do traits vary across ecological scales? A case for trait-based ecology. Ecol. Lett. 13, 838–848. https://doi.org/10.1111/j.1461-0248.2010.01476.x.

Messier, C., Puettmann, K., Chazdon, R., Andersson, K.P., Angers, V.A., Brotons, L., Filotas, E., Tittler, R., Parrott, L., Levin, S.A., 2015. From management to stewardship: viewing forests as complex adaptive systems in an uncertain world. Conserv. Lett. 8, 368–377. https://doi.org/10.1111/conl.12156.

Messier, J., McGill, B.J., Enquist, B.J., Lechowicz, M.J., 2017. Trait variation and integration across scales: is the leaf economic spectrum present at local scales? Ecography 40, 685–697. https://doi.org/10.1111/ecog.02006.

Miller, J.D., Safford, H.D., Crimmins, M., Thode, A.E., 2009. Quantitative evidence for increasing forest fire severity in the Sierra Nevada and southern Cascade Mountains, California and Nevada, USA. Ecosystems 12, 16–32. https://doi.org/10.1007/s10021-008-9201-9.

Moles, A.T., Falster, D.S., Leishman, M.R., Westoby, M., 2004. Small-seeded species produce more seeds per square metre of canopy per year, but not per individual per lifetime. J. Ecol. 92, 384–396. https://doi.org/10.1111/j.0022-0477.2004.00880.x.

Morris, J.L., Cottrell, S., Fettig, C.J., Hansen, W.D., Sherriff, L., Carter, V.A., Clear, J.L., Clement, J., Derose, R.J., Hicke, J.A., Higuera, P.E., Mattor, K.M., Seddon, A.W.R., Stednick, J.D., Seybold, S.J., Sepp, H.T., 2016. Managing bark beetle impacts on ecosystems and society : priority questions to motivate future research. J. Appl. Ecol. 54, 750–760. https://doi.org/10.1111/1365-2664.12782.

Nitschke, C.R., Innes, J.L., 2008. A tree and climate assessment tool for modelling ecosystem response to climate change. Ecol. Model. 210, 263–277. https://doi.org/10.1016/j.ecolmodel.2007.07.026.

Oyler, J.W., Ballantyne, A., Jencso, K., Sweet, M., Running, S.W., 2015. Creating a topoclimatic daily air temperature dataset for the conterminous United States using homogenized station data and remotely sensed land skin temperature. Int. J. Climatol. 35, 2258–2279. https://doi.org/10.1002/joc.4127.

Pan, Y., Chen, J.M., Birdsey, R., McCullough, K., He, L., Deng, F., 2011. Age structure and disturbance legacy of North American forests. Biogeosciences 8, 715–732. https://doi.org/10.5194/bg-8-715-2011.

Parks, S.A., Abatzoglou, J.T., 2020. Warmer and drier fire seasons contribute to increases in area burned at high severity in western US forests from 1985 to 2017. Geophys. Res. Lett. 47, e2020GL089858 https://doi.org/10.1029/2020GL089858.

Parks, S.A., Holsinger, L.M., Miller, C., Nelson, C.R., 2015. Wildland fire as a self-regulating mechanism: the role of previous burns and weather in limiting fire progression. Ecol. Appl. 25, 1478–1492. https://doi.org/10.1890/14-1430.1.

Parks, S.A., Parisien, M.-A., Miller, C., Holsinger, L.M., Baggett, L.S., 2018. Fine-scale spatial climate variation and drought mediate the likelihood of reburning. Ecol. Appl. 28, 573–586. https://doi.org/10.1002/eap.1671.

Pebesma, E., 2018. Simple features for R: standardized support for spatial vector data. The R J. 10, 439–446.

Pierce, D., 2017. ncdf4: Interface to Unidata netCDF (Version 4 or Earlier) Format Data Files.

Prichard, S.J., Stevens-Rumann, C.S., Hessburg, P.F., 2017. Tamm review: shifting global fire regimes: lessons from reburns and research needs. For. Ecol. Manag. 396, 217–233. https://doi.org/10.1016/J.FORECO.2017.03.035.

Prichard, S.J., Kennedy, M.C., Andreu, A.G., Eagle, P.C., French, N.H., Billmire, M., 2019. Next-generation biomass mapping for regional emissions and carbon inventories: incorporating uncertainty in wildland fuel characterization. J. Geophys. Res.: Biogeosciences 124, 3699–3716. https://doi.org/10.1029/2019JG005083.

Rabin, S.S., Melton, J.R., Lasslop, G., Bachelet, D., Forrest, M., Hantson, S., Kaplan, J.O., Li, F., Mangeon, S., Ward, D.S., Yue, C., Arora, V.K., Hickler, T., Kloster, S., Knorr, W., Nieradzik, L., Spessa, A., Folberth, G.A., Sheehan, T., Voulgarakis, A., Kelley, D.I., Prentice, I.C., Sitch, S., Harrison, S., Arneth, A., 2017. The Fire Modeling Intercomparison Project (FireMIP), phase 1: experimental and analytical protocols with detailed model descriptions. Geosci. Model Dev. (GMD) 10, 1175–1197. https://doi.org/10.5194/gmd-10-1175-2017.

Radeloff, V.C., Helmers, D.P., Kramer, H.A., Mockrin, M.H., Alexandre, P.M., Bar-Massada, A., Butsic, V., Hawbaker, T.J., Martinuzzi, S., Syphard, A.D., Stewart, S.I., 2018. Rapid growth of the US wildland-urban interface raises wildfire risk. In: Proceedings of the National Academy of Sciences. https://doi.org/10.1073/pnas.1718850115, 201718850–201718850.

Rammer, W., Seidl, R., 2015. Coupling human and natural systems: simulating adaptive management agents in dynamically changing forest landscapes. Global Environ. Change 35, 475–485. https://doi.org/10.1016/j.gloenvcha.2015.10.003.

Rammer, W., Seidl, R., 2019. A scalable model of vegetation transitions using deep neural networks. Methods Ecol. Evol. 10, 879–890. https://doi.org/10.1111/2041-210X.13171.

Rammig, A., Bebi, P., Bugmann, H., Fahse, L., 2007. Adapting a growth equation to model tree regeneration in mountain forests. Eur. J. For. Res. 126, 49–57. https://doi.org/10.1007/s10342-005-0088-0.

Reineke, L.H., 1933. Perfecting a stand-density index for even aged forests. J. Agric. Res. 46, 627–638.

Rose, K.C., Graves, R.A., Hansen, W.D., Harvey, B.J., Qiu, J., Wood, S.A., Ziter, C., Turner, M.G., 2017. Historical foundations and future directions in macrosystems ecology. Ecol. Lett. 20, 147–157. https://doi.org/10.1111/ele.12717.

Ruefenacht, B., Finco, M.V., Nelson, M.D., Czaplewski, R., Helmer, E.H., Blackard, J.A., Holden, G.R., Lister, A.J., Salajanu, D., Weyermann, D., Winterberger, K., 2008. Conterminous U.S. and Alaska forest type mapping using forest inventory and analysis data. Photogramm. Eng. Rem. Sens. 74, 1379–1388. https://doi.org/10.14358/PERS.74.11.1379.

Ruess, R.W., Winton, L.M., Adams, G.C., 2021. Widespread mortality of trembling aspen (Populus tremuloides) throughout interior Alaskan boreal forests resulting from a novel canker disease. PLoS One 16, e0250078. https://doi.org/10.1371/journal.pone.0250078.

Sanderson, B.M., Fisher, R.A., 2020. A fiery wake-up call for climate science. Nat. Clim. Change 10, 175–177. https://doi.org/10.1038/s41558-020-0707-2.

Schoennagel, T., Balch, J.K., Brenkert-Smith, H., Dennison, P.E., Harvey, B.J., Krawchuk, M.A., Mietkiewicz, N., Morgan, P., Moritz, M.A., Rasker, R., Turner, M.G., Whitlock, C., 2017. Adapt to more wildfire in western North American forests as climate changes. Proc. Natl. Acad. Sci. 114, 4582–4590. https://doi.org/10.1073/pnas.1617464114.

Schumacher, S., Reineking, B., Sibold, J., Bugmann, H., 2006. Modeling the impact of climate and vegetation on fire regimes in mountain landscapes. Landsc. Ecol. 21, 539–554. https://doi.org/10.1007/s10980-005-2165-7.

Seidl, R., Rammer, W., Scheller, R.M., Spies, T.A., 2012a. An individual-based process model to simulate landscape-scale forest ecosystem dynamics. Ecol. Model. 231, 87–100. https://doi.org/10.1016/j.ecolmodel.2012.02.015.

Seidl, R., Spies, T.A., Rammer, W., Steel, E.A., Pabst, R.J., Olsen, K., 2012b. Multi-scale drivers of spatial variation in old-growth forest carbon density disentangled with lidar and an individual-based landscape model. Ecosystems 15, 1321–1335. https://doi.org/10.1007/s10021-012-9587-2.

Seidl, R., Rammer, W., Spies, T.A., 2014. Disturbance legacies increase the resilience of forest ecosystem structure , composition , and functioning. Ecol. Appl. 24, 2063–2077.

Seidl, R., Honkaniemi, J., Aakala, T., Aleinikov, A., Angelstam, P., Bouchard, M., Boulanger, Y., Burton, P.J., De Grandpré, L., Gauthier, S., Hansen, W.D., Jepsen, J. U., Jõgiste, K., Kneeshaw, D.D., Kuuluvainen, T., Lisitsyna, O., Makoto, K., Mori, A. S., Pureswaran, D.S., Shorohova, E., Shubnitsina, E., Taylor, A.R., Vladimirova, N., Vodde, F., Senf, C., 2020. Globally consistent climate sensitivity of natural disturbances across boreal and temperate forest ecosystems. Ecography 43, 967–978. https://doi.org/10.1111/ecog.04995.

Serra-Diaz, J.M., Maxwell, C., Lucash, M.S., Scheller, R.M., Laflower, D.M., Miller, A.D., Tepley, A.J., Epstein, H.E., Anderson-Teixeira, K.J., Thompson, J.R., 2018. Disequilibrium of fire-prone forests sets the stage for a rapid decline in conifer dominance during the 21st century. Sci. Rep. 8, 6749. https://doi.org/10.1038/s41598-018-24642-2, 6749.

Stanke, H., Finley, A.O., Weed, A.S., Walters, B.F., Domke, G.M., 2020. rFIA: an R package for estimation of forest attributes with the US Forest Inventory and Analysis database. Environ. Model. Software 127, 104664. https://doi.org/10.1016/j.envsoft.2020.104664.

Steel, Z.L., Koontz, M.J., Safford, H.D., 2018. The changing landscape of wildfire: burn pattern trends and implications for California's yellow pine and mixed conifer forests. Landsc. Ecol. 33, 1159–1176. https://doi.org/10.1007/s10980-018-0665-5.

Stenzel, J.E., Bartowitz, K.J., Hartman, M.D., Lutz, J.A., Kolden, C.A., Smith, A.M.S., Law, B.E., Swanson, M.E., Larson, A.J., Parton, W.J., Hudiburg, T.W., 2019. Fixing a snag in carbon emissions estimates from wildfires. Global Change Biol. 25, 3985–3994. https://doi.org/10.1111/gcb.14716.

Tepley, A.J., Thomann, E., Veblen, T.T., Perry, G.L.W., Holz, A., Paritsis, J., Kitzberger, T., Anderson-Teixeira, K.J., 2018. Influences of fire-vegetation feedbacks and post-fire recovery rates on forest landscape vulnerability to altered fire regimes. J. Ecol. 106, 1925–1940. https://doi.org/10.1111/1365-2745.12950.

Turetsky, M.R., Baltzer, J.L., Johnstone, J.F., Mack, M.C., McCann, K., Schuur, E.A.G., 2017. Losing legacies, ecological release, and transient responses: key challenges for the future of northern ecosystem science. Ecosystems 20, 23–30. https://doi.org/10.1007/s10021-016-0055-2.

Turner, M.G., Romme, W.H., Gardner, R.H., Hargrove, W.W., 1997. Effects of fire size and pattern on early succession in Yellowstone National Park. Ecol. Monogr. 67, 411–433.

Von Bertalanffy, L., 1957. Quantitative laws in metabolism and growth. Q. Rev. Biol. 32, 217–231. https://doi.org/10.1086/401873.

Walker, X.J., Rogers, B.M., Baltzer, J.L., Cumming, S.G., Day, N.J., Goetz, S.J., Johnstone, J.F., Schuur, E.A.G., Turetsky, M.R., Mack, M.C., 2018. Cross-scale controls on carbon emissions from boreal forest megafires. Global Change Biol. 24, 4251–4265. https://doi.org/10.1111/gcb.14287.

Westerling, A.L., 2016. Increasing western US forest wildfire activity: sensitivity to changes in the timing of spring. Phil. Trans. Biol. Sci. 371, 20150178 https://doi.org/10.1098/rstb.2015.0178.

Westerling, A.L., Turner, M.G., Smithwick, E.A.H., Romme, W.H., Ryan, M.G., 2011. Continued warming could transform Greater Yellowstone fire regimes by mid-21st century. Proc. Natl. Acad. Sci. 108, 13165–13170. https://doi.org/10.1073/pnas.1110199108.

Wickham, H., Ruiz, E., 2020. Dbplyr: A "Dplyr" Back End for Databases.

Wickham, H., Averick, M., Bryan, J., Chang, W., McGowan, L.D., François, R., Grolemund, G., Hayes, A., Henry, L., Hester, J., Kuhn, M., Pedersen, T.L., Miller, E., Bache, S.M., Müller, K., Ooms, J., Robinson, D., Seidel, D.P., Spinu, V., Takahashi, K., Vaughan, D., Wilke, C., Woo, K., Yutani, H., 2019. Welcome to the {tidyverse. J. Open Source Softw. 4, 1686. https://doi.org/10.21105/joss.01686.

Williams, A.P., Cook, B.I., Smerdon, J.E., Bishop, D.A., Seager, R., Mankin, J.S., 2017. The 2016 Southeastern U.S. drought: an extreme departure from centennial wetting and cooling. J. Geophys. Res. Atmos. 122 https://doi.org/10.1002/2017JD027523, 10,888-10,905.

Williams, A.P., Cook, E.R., Smerdon, J.E., Cook, B.I., Abatzoglou, J.T., Bolles, K., Baek, S. H., Badger, A.M., Livneh, B., 2020. Large contribution from anthropogenic warming to an emerging North American megadrought. Science 368, 314–318. https://doi.org/10.1126/science.aaz9600.

Williams, A.P., Livneh, B., McKinnon, K.A., Hansen, W.D., Mankin, J.S., Cook, B.I., Smerdon, J.E., Varuolo-Clarke, A.M., Bjarke, N.R., Juang, C.S., Lettenmaier, D.P., 2022. Growing impact of wildfire on western US water supply. Proc. Natl. Acad. Sci. U.S.A. 119, e2114069119 https://doi.org/10.1073/pnas.2114069119.